Springer

Available online at https://link.springer.com/journal/42241
http://www.jhydrodynamics.com
Journal of Hydrodynamics, 2022, 34(6): 1121-1133
https://doi.org/10.1007/s42241-022-0077-5

Measurement and characterization of bulk nanobubbles by nanoparticle tracking analysis method

Xiao-tong Ma, Ming-bo Li*, Chao Sun
Center for Combustion Energy, Key Laboratory for Thermal Science and Power Engineering of Ministry of Education, Department of Energy and Power Engineering, Tsinghua University, Beijing 100084, China

(Received June 21, 2022, Revised July 26, 2022, Accepted August 2, 2022, Published online December 14, 2022)

Abstract: The size of the bulk nanobubbles (typically 100 nm-200 nm in diameter) is below the optical resolution of the typical microscopes, which makes it difficult to make a direct observation of them and differentiate between the nanoparticles and the nanobubbles. In this work, a nanoparticle tracking analysis (NTA) system is developed for tracking and sizing the bulk nanobubbles, and more broadly, the Brownian diffusing particles. We demonstrate the capabilities of the NTA in characterizing the nanoparticles through systematic validation of accuracy and resolution. We particularly exhibit its unique advantages in detecting the polydisperse nanoparticle populations. Then the nucleation and the thermodynamic stability of the bulk nanobubbles are systematically studied by the NTA system. The bulk nanobubbles smaller than 600 nm in size are generated via the ultrasonication method. It is shown that both the ultrasonic cavitation treatment time and amplitude, essentially, the energy input, favor the nucleation of the bulk nanobubbles with a more concentrated size distribution, a higher concentration, and a smaller hydrodynamic size. The temperature dependence of the bulk nanobubbles over a wide range from 25°C to 70°C is explored. It is found that the nanobubble first shrinks in size significantly and then the size keeps approximately constant with the increasing temperature, showing a narrow size distribution. The transition temperature is around 45°C. Further, as an open system, the NTA is a potential tool in the study of the dynamic behavior of the bulk nanobubbles *in situ*, such as the coalescence and the collapse.

Key words: Nanoparticle tracking analysis, bulk nanobubble, light scattering, hydrodynamic size, number concentration

Introduction

The nanobubbles are the nanoscale gaseous domains, either suspended in solutions, namely the bulk nanobubble, or adsorbed on the submersed substrates, namely the surface nanobubble[1]. In recent years, they have attracted increasing research interests arising from pivotal scientific challenges and potential applications. The bubble shrinking to the nanoscale has a series of unique advantages, such as the high specific surface area, the high mass transfer efficiency, and the good biocompatibility. Many studies have focused on their roles in practical applications, such as the flotation, the cleaning, the medicine, the aquaculture, the water treatment and the environmental remediation[2-4].

The long-term stability is a puzzling issue for the nanobubbles, as in contract with the classic Epstein-Plesset theory[5], extensively verified experimentally for a century. Theoretically, as a simple estimate, the small bubbles with a radius of curvature of less than 500 nm would disappear in the water within a few milliseconds or less, driven by the tremendous Laplace pressure $\Delta P = 2\gamma / R$, where γ is the surface tension coefficient. What is surprising is that a manifold of experiments show that the nanobubbles could persist in liquids for days and weeks[6-7]. So far the apparent paradox between the theoretical prediction and the experimental fact is still controversial and challenging. Particularly, the nanoscopic bubbles are difficult to be directly observed with current methods due to the optical resolution limit. Moreover, there is no technology available to explicitly identify the gaseous content inside the bubble, to be distinguished with the nanoparticles or the nanodroplets.

The existence of the nanobubbles of spherical cap-shaped surface has confirmed experimentally and widely accepted. The key to identify them is to recognize their topography and chemical composition with complementary imaging techniques[8], such as the

Project supported by the National Natural Science Foundation of China (Grant Nos. 11988102, 91852202), the Tencent Foundation through the XPLORER PRIZE.
Biography: Xiao-tong Ma (1996-), Female, Ph. D. Candidate,
E-mail: maxt19@mails.tsinghua.edu.cn
Corresponding author: Ming-bo Li,
E-mail: mingboli@mail.tsinghua.edu.cn

atomic force microscopy (AFM), the x-ray reflectivity measurement, the total internal reflection fluorescence microscopy (TIRF), the Fourier transform infrared spectrometer (FTIR) and even the optical microscopy. Their stability has been explained theoretically with various mechanisms, with a growing consensus that the pinning of the three-phase contact line and the local supersaturation contribute to the stability collectively[9-10].

In contrast, the mystery of the bulk nanobubbles is a much more challenging issue concerning their movement and the random Brownian motion incessantly occurring in the liquids. Although there is not yet a technique to image them directly, there are a number of ways to characterize the physical properties of the bulk nanobubbles. The solution of the conundrum in the observation of the bulk nanobubbles is inspired by the visual experiences for the surface nanobubbles. The high-resolution electron microscopy is a fundamental approach to detect the nanobubbles. It has been demonstrated that the cryogenic scanning electron microscopy (SEM)[11] and the liquid transmission electron microscopy (TEM)[12] can be applied to detect the bulk nanobubbles indirectly. However, it is limited by the rigorous requirements on the samples and the test conditions[13]. The holography and phase-contrast microscopy is an alternative to acquire the phase information, to distinguish the gaseous bubbles from others in terms of the refractive index (RI)[14]. In addition, the density and the chemical composition of the bulk nanobubbles are tested with the techniques of the resonant mass measurement[15] and the vibrational spectroscopy[16-17]. The methods mentioned above help the understanding of the bulk nanobubbles. Nevertheless, the obtained results are not widely recognized, due to a lack of systematic verification and direct evidence of the existence of the bulk nanobubbles.

The dynamic light scattering (DLS) is a powerful and user-friendly technique for the analysis of the nanoparticles. Particularly, it is a favored technique for determining the size of the bulk nanobubbles routinely. Despite being widely used and even with its boosting of the fields of the nanobubbles in the earlier years, the DLS has several drawbacks, primarily inherent in the measuring principles of the method[8]. The size of the particle size is decided by the fluctuations of the scattered light intensity caused by the Brownian motion of the particles. The fluctuations of the light scattering signal are the collective behavior of all particles in the bulk. The technique is rather sensitive to the presence of large particles theoretically due to the fact that the intensity of the scattered light is proportional to the sixth power of the diameter. This may therefore overestimate the size of the nanoparticle samples, especially, those of high polydispersity.

The nanoparticle tracking analysis (NTA) method can overcome this drawback by detecting the size of an individual nanoparticle and the concentration of a sample, and it is widely used in many fields[18-20]. While the technique is still unable to directly and optically determine the nano-entities, its scattered light spots do reflect the position and the Brownian motion of each particle in the field of view, enabling "the visual-like" measurements. Several NTA measurements over-rely on the "black box" characterization techniques, in the determination of the size distributions, with no proofs that the observed objects truly are nanobubbles. We should not only try to improve the accuracy and the resolution of the techniques but also try to make the *in-situ* measurement possible. An open-ended, real-time and convenient measuring equipment is desirable. It is vital to monitor the response of the bulk nanobubbles according to the kinds of physical perturbations and further tune and control the properties of the nanobubbles.

In this paper, we built an open-ended NTA system for characterizing the bulk nanobubbles under multifarious experimental conditions. The accuracy and the resolution of the NTA system are validated using different types of standard nanoparticles of the nominal diameter, compared with the results of the DLS and SEM techniques, ensuring the reliability of the measurements. Then the bulk nanobubbles produced by the ultra-sonication with various times and amplitudes are measured by the NTA system to study the generation and nucleation processes. Meanwhile, the effects of the wide range temperatures on the stability of the bulk nanobubbles are also discussed in detail, to provide some insight into the researches of the response of the bubbles to the physical perturbations.

1. Materials and methods

1.1 *Materials*

Gold nanoparticle suspensions with a density of ~1 000 kg/m^3, nominally sized 20 nm, 60 nm, 100 nm, 150 nm and 200 nm, are purchased from Dk Nano technology Co., Ltd, (Beijing, China). Aqueous dispersion of the polystyrene spheres with various nominal diameters of 60 nm, 100 nm, 150 nm and a density of ~1 050 kg/m^3 are obtained from Thermo Fisher (Waltham MA, USA), primarily for quality control and verification purposes. Detailed information on the nanoparticles used is shown in Table 1. All samples are diluted to a certain concentration with ultrapure water, produced from a Millipore Milli-Q system (Merck, Millipore, Germany). The ultrapure

water has an electrical conductivity of 18.2 MΩ·cm and a pH value of 6.5 at 25℃. Then these particles are mixed to prepare a series of suitable bimodal particle suspensions. All glassware and sample cells used in the experiments are cleaned by ethanol (> 99%, AR, Titan, China) and ultrapure water ultrasonically for at least 15 min in turn. Before any measurements, the pure water is tested by both the dynamic light scattering and nanoparticle tracking analysis techniques, assuring that no detectable nano-scale contaminants are present.

1.2 *NTA system*

The schematic view of the nanoparticle tracking analysis system built in our lab is shown in Fig. 1. Structurally, it consists of three parts, namely, a microfluidic sample cell, a laser, and a dark-field microscope equipped with a high-speed camera. At the center of this measuring system is a microfluidic cell, making of two sheets of quartz glass with a good light transmittance and a fluoroelastomer spacer, creating an enclosed space, as depicted in Fig. 1(a). The upper cover plate is designed to allow both the laser beam and the fluid to enter the sample space from different sides. The three-layer assembly is fastened with four nylon bolts, and can be easily disassembled for cleaning. The sample, of approximately ~1 mL, is introduced from the inlet into the chamber with a glass dropper via the PTFE inverted-taper connector and the PTFE tube, and then discharged through the outlet on the other side (see Fig. 1(b)). The hexagonal-like sample chamber has a height of 500 μm and a maximum width (circumscribed circle) of 20 mm. The inlet and the outlet of the micro-channel are located at the corners to minimize the trapping of air bubbles during loading. In addition, the cell is roofed with a detachable polyimide electrothermal film, equipped with a PID control, for the purpose of controlling the temperature of the sample during the measurements. Owing to the lack of a cooling module, the applicable temperature ranges from 25℃ (room temperature) to 70℃.

Table 1 Detailed information of the nanoparticle suspensions

Sample	Material	Nominal diameter/nm
Au60	Gold	60 ± 4
Au100	Gold	101 ± 4
Au150	Gold	152 ± 4
PE60	Polystyrene	60 ± 3
PE100	Polystyrene	102 ± 3
PE150	Polystyrene	147 ± 3

To observe the nanoparticles within the chamber, a 150mW laser beam (attenuated if necessary) of a wavelength of 520 nm is reflected multiple times exactly through the prism-like edge into the optical platform. In the experiment, the angle of the Mirror 3 in Fig. 1(c) is adjusted so that the path of the light in the sample after being refracted is almost parallel to the glass-sample interface. Scattering light from the individual nanoparticles in the beam path can be visualized by an inverted optical dark-field microscope (IX73, Olympus, Japan) with an accessory of long working distance objective (×20) and a high-sensitivity CCD camera (xiD, XIMEA, Germany). The images captured in the CCD sensor have effective pixels of 1 936×1 456 with a resolution of 227 nm/pixel.

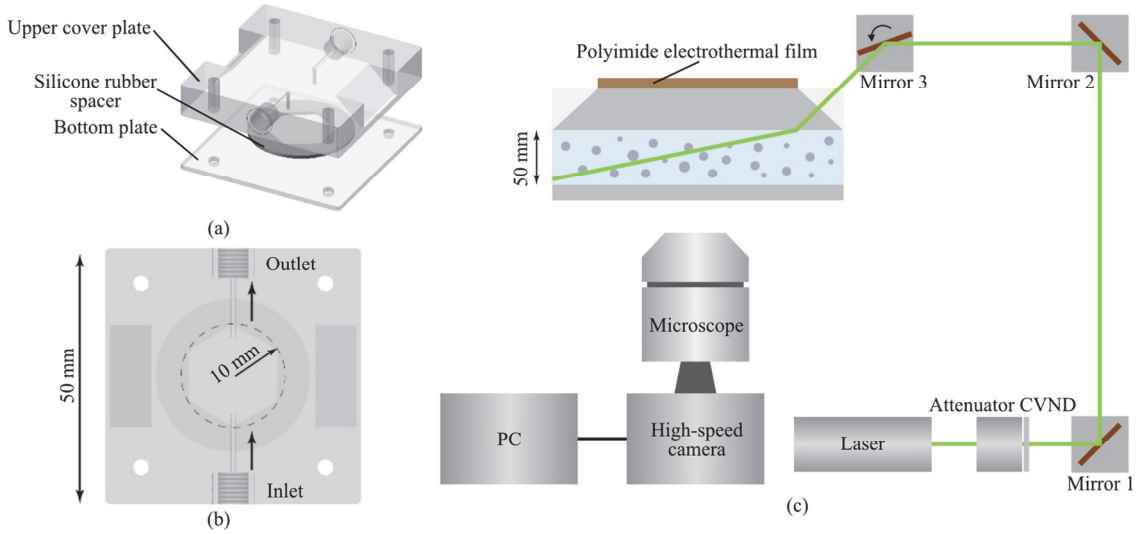

Fig. 1 (Color online) Schematic diagram of the NTA measurement system. (a) Structure of microfluidic sample cell. (b) Top view of channel, the sample is injected from the inlet, remained in viewing area and discharged from the outlet. (c) Overview of the NTA system. The nanoparticles in the suspensions are illuminated by a laser and the light scattering spots are recorded by a microscope with a high-speed camera

Nanoparticles within the laser beam path are seen through the microscope as spots of light. It should be noted that the nanoparticles as the scattered spots are not imaged directly. The size of the nanoparticles is so far below the Rayleigh or Abbe limit that the structure and the morphology could not be resolved through the optical method[21]. In view of the fact that the width of the laser beam is narrower than the observing area of the CCD sensor, an appropriate view is selected in the middle based on the criterion that all nanoparticles in the field are visualized, which is around 350 μm× 180 μm. The visible nanoparticles move freely in the space with a height of around 5.16 μm, which is the depth of the field determined by the objective and the magnification of the microscope. The Brownian motion of the nanoparticles, in the form of scattering bright spots, is recorded at a framerate of 30 frames per second (fps) for a duration of 60 s. Since the intensity of the light scattering depends on the size and the nature of the object being observed, the exposure time is adjusted according to the optical characteristics of the samples.

1.3 *Methodology*

The NTA technology is used to obtain the information of the nanoparticle suspensions, such as the number concentration, the motion trajectory and the size distribution, generally, through four steps: (1) The video capturing, (2) The particle identifying, (3) The particle tracking and (4) The size estimating[22-23]. The measuring processes are described in detail as follows:

Firstly, it is necessary to capture a clear video for the Brownian motion of the nanoparticles in view, which is shown as the scattered spots of light with diffraction patterns. The distinct capture of the nanoparticles is determined by not only the instrumental settings, including the intensity and the orientation of the illumination, the numerical aperture of the objective, and the camera sensitivity, but also a suitable adopted concentration of the particles. In order that the nanoparticles of interest stand out from the diffraction and flare patterns, the video sequence is pre-treated in terms of the background subtraction, the threshold setting and the blurring removal.

Next, the nanoparticles in each frame are identified utilizing the “Find Maximum” method in ImageJ. The working principle is as follows: the local maximum pixel is estimated by searching the eight neighborhoods of each pixel one after another. With the flood-filling algorithm, all pixels are grouped around the respective local maximum and the center of gravity of the regions is identified as the location of the maximum value[23]. Hence, the positions of light scattered spots are identified and marked with yellow cross markers as shown in Fig. 2(a). In addition, there is another alternative way to determine the center of the nanoparticle by using the Gaussian fit of sub-pixel accuracy. However, it is not applicable in all cases. Simultaneously, the bright spots in the selected view could be counted and from which we can obtain the number concentrations within the observing volume. The average and the standard deviation of the number concentrations are calculated from the data of fifteen random images per test. The interactions between particles play an important role in the movements of the particles in the liquid. In order to avoid the interplay between the nanoparticles as much as possible, the concentration of the particles in the solution should not be too high. The upper limit of the detection concentration is determined by two conditions: one is to guarantee that all nanoparticles in the solution are illuminated, and the other is to ensure that the motion trajectories do not overlap. Meanwhile, a high concentration improves the statistical accuracy of the measurements. According to the results of tests and previous studies[18, 21], the sample recommended concentrations should lie between 10^6-10^9 particles/ ml.

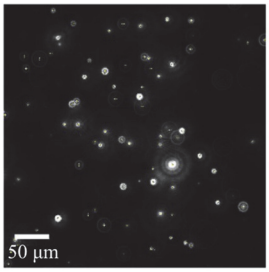

Fig. 2(a) Image captured by the CCD sensor with a microscope

After identifying the individual nanoparticles in each frame, it is essential to connect the positions in a bunch of image sequences, which could be implemented through the NanoTrackJ[23] plugin in the ImageJ. The crux of the algorithm lies in determining whether two particles in subsequent frames are matched accurately. The tracking algorithm interconnects the positions of the particle only if there is one and only one particle that corresponds to it in the previous frame. After being connected successfully, two centers are considered to belong to a same particle and the positions of the two centers represent the distance covered by the particle during the time interval. As shown in Fig. 2(b), the thermal Brownian motion of the individual nanoparticle is tracked frame by frame over a period of time and the trajectory of typical nanoparticles is depicted as the yellow line. Specifically, the search radius of the trajectory is estimated by the maximum expected diffusion coefficient, $r = 3\sqrt{\pi D_{\max} \Delta t}$, providing that the temperature and the viscosity are fixed. It is important to ensure that the distance between two particles in two frames is

within the search radius. Notably, too large or too small search radius will result in shorter track lengths, causing errors to some extent.

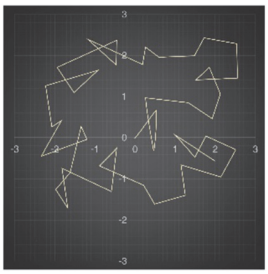

Fig. 2(b) (Color online) Brownian motion of nanoparticle is depicted as the yellow trajectories

The diffusion coefficient is calculated by the trajectory of the particle, independent of any other parameters. When a nanoparticle diffuses in one dimension, the measured position $X[n]$ at the discrete time point $t_n = \Delta t$ and the covariance estimator is given by

$$\hat{D} = \frac{\overline{\Delta X_n \Delta X_n}}{2\Delta \mathrm{t}} + \frac{\overline{\Delta X_n \Delta X_{n+1}}}{\Delta \mathrm{t}} \tag{1}$$

where $\Delta X_n = x[n] - x[n-1]$ and the second term in the right side is an estimator for the localization noise. On the basis of the mean squared displacement of the particles and the time lags per step, we could obtain the diffusion constant of individual nanoparticles. Theoretically, once the precise diffusion constant is obtained, the hydrodynamic diameter of the particle under the Brownian motion can be estimated based on the Stokes-Einstein equation

$$d = \frac{k_B T}{3\pi\eta D} \tag{2}$$

where D is the diffusion constant, k_B is the Boltzmann constant, T is the temperature and η is the viscosity of the suspensions. In this way, the histogram could be constructed by weighting each diameter by the individual track length instead of the complete track. Besides, there is another alternative way to gain the size distribution. Different from a simple method, a maximum likelihood approach takes the finite number of steps of the tracked particles into account, which offers easier identified modal values in the histogram[22]. Once the size distribution of the nanoparticles is derived, the estimation of the mean diameter is straightforward.

1.4 *Bulk nanobubbles generation*

Bulk nanobubbles suspensions are generated by a liquid ultrasonic processor (VCX 750 W, 20 kHz, Sonics and Materials, USA) based on the ultrasonic cavitation method[24-25]. In all experiments, 100 mL of pure water stored in the clean glass beaker is processed by the titanium probe (0.01905 m in diameter) with varying ultrasonic amplitude and time. Prior to the generation of the bulk nanobubbles, the titanium probe is cleaned with the ethanol and pure water for at least 5 min ultrasonic treatment to reduce the fall-off contaminants. In order to maintain the temperature of the suspensions at 25°C, the glass beaker is immersed in a water recirculating cooler equipment (PolyScience PP15r-40, USA) during the ultrasonic process. To diminish the severe temperature fluctuations, a pulse-working mode is adopted with 20 s ON and 10 s OFF and the ultrasonic time is determined by the ON-state treatment. The bulk nanobubble suspensions produced are kept in the airtight glass vials for further measurements.

1.5 *DLS and SEM*

The dynamic light scattering (DLS) measurements are performed with a Zetasizer NanoZSE system (ZEN3700, Malvern Instruments, UK) equipped with a 633 nm He-Ne laser. The non-invasive backscatter detection is employed to collect the signal of the intensity at an angle of 173°. 1 mL sample suspension is loaded into an original cuvette and then measured after around 5 min. The measurements are conducted with an automatic attenuator under the temperature of 25°C (unless explicitly stated otherwise). The refractive index depends on the properties of the respective samples. At 25℃, the refractive index of the solvent (water) is set as 1.33. Based on the signal of the scattered intensity detected, the size distribution, the average diameter, and the polydispersity index are calculated through the autocorrelation function. Each sample is tested six times at least. A field emission scanning electron microscope (SEM, Gemini SEM 300, Zeiss, Germany) is used to characterize the appearance and the size of the nanoparticles. The sample suspensions are dropped on a silicon wafer and dried in the oven for 10 min around 50°C. With the dry samples, the silicon wafer is fixed on the holder with an electrically conducting double-sided tape (Plano, Wetzlar, Germany). For samples with poor electrical conductivity, such as the polystyrene nanoparticles used in this study, the samples need to be coated with an ultrathin layer of gold by high-vacuum evaporation using a sputtering coater (Model S150RTL, Cowaq Company, Hertfordshire, UK) to increase the electrical conductivity. All measurements are conducted under vacuum and at a room temperature of around 25°C.

2. Results and discussions

2.1 *Accuracy validation of NTA system*

In this section, we will demonstrate the capacity of the developed NTA system to identify and determine the size of any kind of nanoparticles. To validate the accuracy, two common samples, Au and PE nanoparticles, are measured and characterized by using the NTA system. Although the physical properties of Au and PE nanoparticles are different from that of the nanobubbles, what really matters is the characteristics of the Brownian motion, which mainly depend on the temperature and the size of the particles. Hence, these two kinds of monodispersed standard nanoparticles with a nominal diameter could be used for validating the accuracy of the NTA measurements. Simultaneously, the DLS and the SEM, two frequently-used techniques, are applied to measure the size of these nanoparticle samples for comparison. All diagrams of size distribution are the relative intensity I of nanoparticles with different diameter d.

For the SEM measurements, there are some requirements for the sample preparation with regard to the dimension, the electrical conductivity and the phase state. Firstly, the samples have to be small enough to match the limited specimen stage and the vacuum space.

Secondly, the high electrical conductivity and the high stability are needed to withstand the large energy electron beam and the high vacuum environments. Thirdly, the sample should be dried or frozen as imaging occurs under a vacuum, implying that the SEM is not very suitable for the characterization of the droplets and the bubbles. Standard samples of the nanoparticles with a nominal diameter are observed by the SEM. The particular preparations for the suspensions of the gold nanoparticles and the polystyrene microspheres are shown in Section 1.5.

The SEM images of the samples Au60, Au100 and Au150 are shown in Fig. 3(a), where with the gold nanoparticles, a near-spherical morphology with almost uniform size is observed. The size of nanoparticles in the SEM images is analyzed and counted using image processing techniques. It is found in figure Fig. 3(b) that the measurement results follow the unimodal distribution with the peak at 60 nm, 100 nm and 150 nm, which are respectively in accordance with the nominal typical diameter of the samples. Correspondingly, three polyethylene microspheres (PE60, PE100 and PE150) with the nominal sizes of 60 nm, 100 nm and 150 nm are characterized, as shown in Fig. 3(a). Similar spherical shapes are

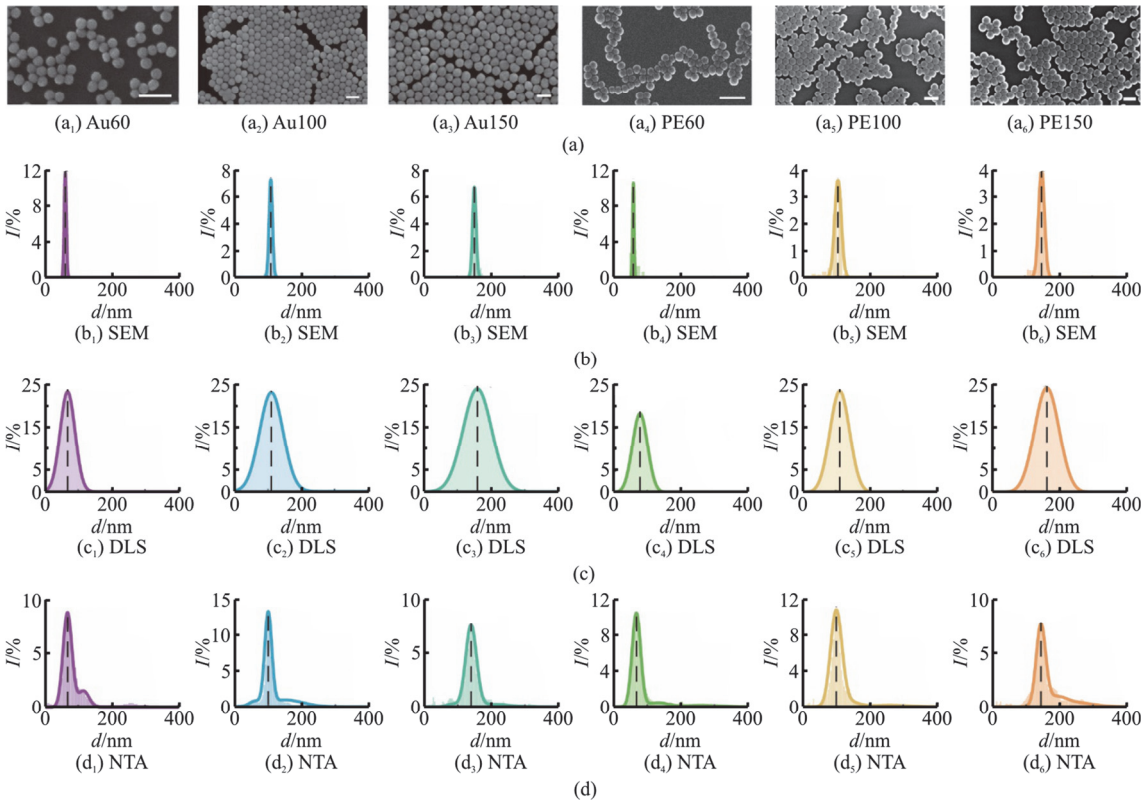

Fig. 3 (Color online) Accuracy validation of size distribution measurements applying gold nanoparticles and polystyrene spheres with varying diameter. (a) Images of standard nanoparticles captured by SEM (scale bar, 200 nm). (b) Size distribution calculated by the SEM observation. (c) Size distribution measured by the DLS techniques. (d) Size distribution measured by the NTA techniques. The dashed lines in the figures denote the nominal diameter of nanoparticles

observed in the SEM images and the typical sizes (see Fig. 3(b)) agree well with the given values. From the direct visualization and characterization, it is confirmed that the size of these nanoparticle samples deviates slightly from the corresponding nominal one, and more importantly, the real distribution of these samples is obtained.

Different from the SEM method, both the DLS and NTA methods are used for obtaining the hydrodynamic dimensions of the nanoparticles freely suspended in the solution, namely, the spherically-assumed Brownian particles, rather than the real dimensions. Those two techniques rely on the characteristic of the Brownian motion of the nanoparticles in liquids and the diameter can be calculated based on the Stokes-Einstein equation. It should be noted that the translation diffusion coefficient is also influenced by some other factors, including the topology and the chemical ordering of the particle surface as well as the ionic strength and the ionic composition of the medium. However, the work is limited in comparing with the temperature and the particle size. Apart from the same theoretical principle, there are a number of similarities between the DLS and the NTA, including the non-invasive and real-time nature and the wide range of concentration measurements, which are appropriate for free-moving nano-entities in liquid. Nevertheless, there is a most significant difference between them, that is the way to obtain the diffusion coefficient, a critical parameter in the Stokes-Einstein equation. As mentioned above, the individual nanoparticles are tracked and analyzed independently in the NTA method, whereas in the DLS method, all light signals scattered by the particles are processed collectively. After the samples are diluted to certain concentrations, they are characterized by these two methods. To avoid the additional effect of the time delay on the particle stability, the two measurements are performed almost simultaneously.

Figure 3(c) shows the size distribution profiles of the gold nanoparticles and the polystyrene microspheres with nominal diameters of 60 nm, 100 nm and 150 nm measured by the DLS technique. Generally, the typical peaks are slightly larger than the diameter of the nanoparticle samples estimated by the SEM, which could be ascribed to the diversity between the hydrodynamic diameter in the liquid and the size of the bare particles on the solid sample stage. Compared to the DLS measurements, the results obtained by the NTA system in Fig. 3(d) have smaller mean diameters featuring narrow size distributions. This difference may arise from the difference of the statistical approach between the NTA and the DLS. When the nanoparticles are in the Brownian motion freely in the liquids, the smaller particles move more rapidly, even in and out of the field of view, which leads to a repeated counting of the tiny particles and then to the smaller number-weighted peak size value. Besides, Mie scattering occurs when the size of the nanoparticles is within or comparable to the wavelength of the incident light. Based on the Rayleigh approximation. for Mie scattered particles, the intensity of the scattered light radiation depends strongly upon the wavelength and the size of the particle. With the fixed wavelength of light, and with the intensity of the scattered light according to the sixth power of the size of the particles, the DLS is susceptible to the larger particles in the heterodisperse system. Owing to the nature of the DLS (intensity-weighted) method, the size is measured with a bias towards the large particles and thus larger mean diameters are obtained than those obtained by the NTA method. Overally, the size distribution of the gold nanoparticles and the polystyrene microspheres could be characterized by the NTA system accurately.

2.2 *Resolution evaluation of NTA system*

The nanoparticles suspended in a homogeneous sample may be polydisperse or even heterogeneous, with different peak sizes. With limited information about the nanoparticles in the sample, it is significant for a technique to distinguish the particle populations that differ in size, namely, the resolution. In order to assess the resolution performance of the NTA technique, the gold nanoparticles with different peak sizes (20/60 nm, 20/100 nm, 20/150 nm, 60/100 nm, 60/150 nm and 100/150 nm) are mixed at a certain concentration ratio. These mixtures are characterized by the NTA system, and the results are compared to those of the DLS, as shown in Fig. 4. The left y-axis represents the number concentration N_b of nanoparticles at any given diameter obtained by NTA (number-weighed), while the right y-axis represents the relative intensity I scattered by nanoparticles versus the corresponding size measured by DLS (intensity-weighed).

It can be seen from Figs. 4(a)-4(c) that with both the NTA and the DLS, the typical bimodal peaks can be recognized for these three mixed-nanoparticle suspensions, 20/60 nm, 20/100 nm and 20/150 nm. In particular, the DLS exhibits clear advantages in resolving the size of small particles, e.g., below 50 nm. However, for the nanoparticles with small differences in size, the disadvantage of the DLS technology is prominent, and it is difficult to resolve and separate the two peak sizes, as shown in Figs. 4(d)-4(f). There is only a single peak identified by the DLS measurement for the mixtures Au60/100, Au60/150 and Au100/150 (Table 2). The location of the peak depends on the concentration of the two particles, namely, the intensity of the scattered light. In contrast, with the NTA, the two-size populations in all mixtures

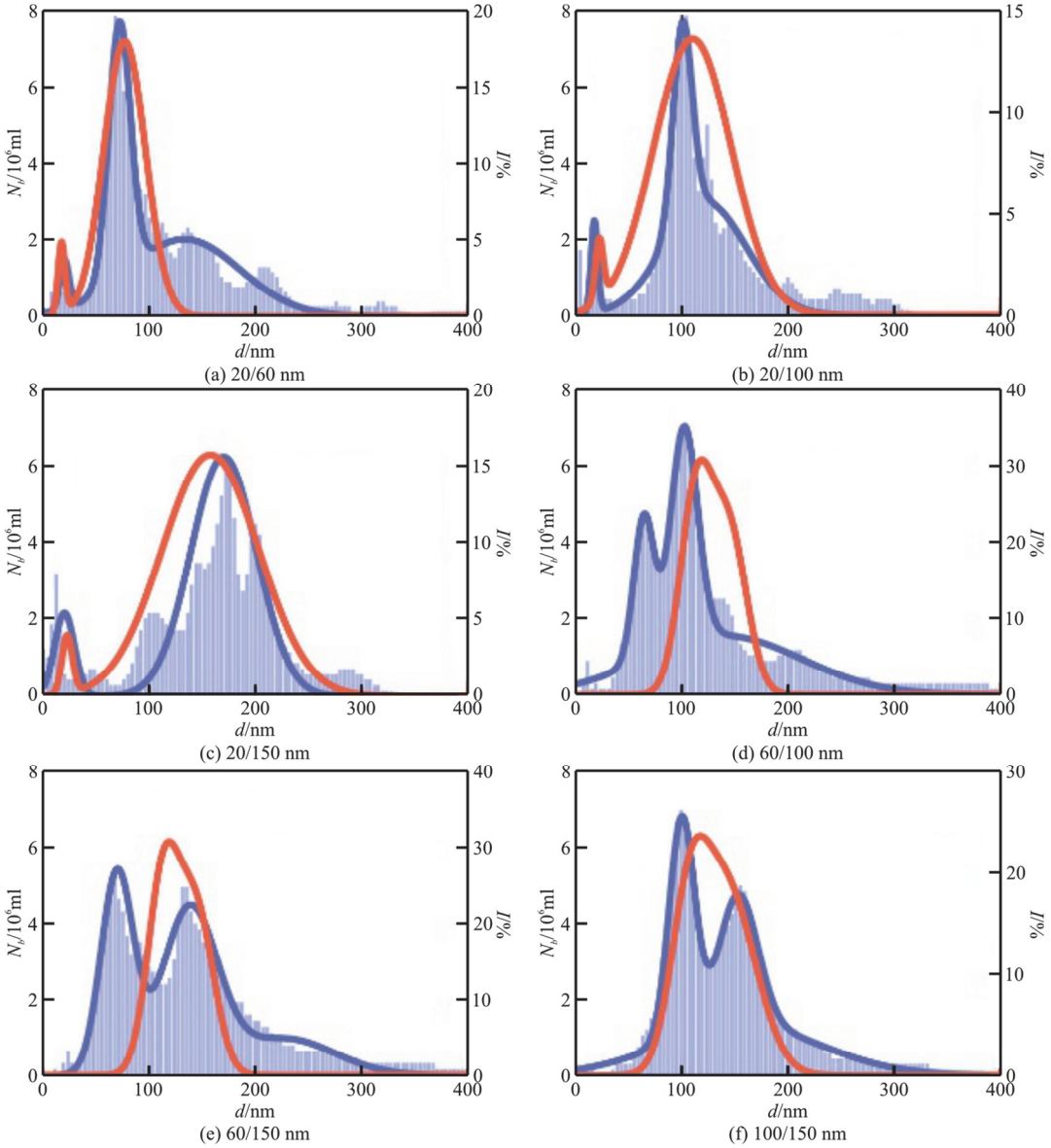

Fig. 4 (Color online) Resolution evaluation of the DLS (intensity-weighted) and the NTA (number-weighted) techniques using gold nanoparticles mixtures with different sizes. (a)-(f) Size distribution of gold nanoparticles mixtures measured by the two complementary techniques, DLS and NTA

can be clearly distinguished and the bimodal size distributions can be delineated accurately. The discrepancy may be originated from the bias of the DLS for larger particles. The light scattered by the spherical particles suspended in a homogeneous non-absorbing medium conforms to the Mie-scattering formalism, suggesting that the scattered light intensity of any particle is proportional to the sixth power of its diameter. The presence of large-sized nanoparticles obscures the scattered light of the small-sized nanoparticles coexisting in the polydisperse system during the measurements.

The characteristic performance of the NTA system is also related to the practical working range, which is primarily determined by the size and the concentration of the nanoparticles. The lower limit of the detection is based upon the properties of the scattering light and the sensitivity of the CCD sensor. For our

Table 2 Size distribution of polydisperse gold nanoparticles obtained from NTA and DLS measurements

Sample	DLS/nm		NTA/nm	
	Peak 1	Peak 2	Peak 1	Peak 2
Au20/60	17±5	76±27	20±6	72±14
Au20/100	22±5	110±52	18±4	10±12
Au20/150	23±7	157±64	18±6	177±37
Au60/100	104±21	-	65±13	103±17
Au60/150	114±22	-	70±21	139±37
Au100/150	142±38	-	101±17	154±26

NTA system, the nanoparticles as small as ~20 nm in diameter could be detected (see Figs. 2(a)-2(c)). It is found experimentally that, for smaller nanoparticles, with the NTA, the individual peaks could not be observed, suggesting that 20 nm is the lower limit of detection. On the other hand, it poses some challenges to measure the large particles. When the radius of the nano-entities approaches and exceeds ~1 μm, the obtained diffusion coefficient could be influenced by the fact whether the Brownian motion or the buoyancy and sedimentation force is dominated. In addition, the intensity of the scattered light increases significantly owing to the large size of the particles. The diffraction rings appear around the large particles, leading to an incorrect centering identity. In view of the precision and the repeatability of the measurements, the effective upper limit of quantification is approximate ~1 μm[21].

2.3 *Effect of ultrasonication on bulk nanobubble nucleation*

We next use the developed NTA system to characterize the bulk nanobubbles in terms of the size distribution and the number concentration, as well as to conduct a preliminary study of the stabilization mechanism of the bulk nanobubbles. We start with the intrinsic nucleation of the bulk nanobubbles in pure water during the ultrasonication. The bulk nanobubbles may originate from the small vapor-filled cavities in the liquid when the static pressure of the water reduces to a level below the vapour pressure, for the cavitation inception. When applying an acoustic field, both the inertial cavitation and the non-inertial cavitation occur simultaneously[26]. If the acoustic intensity is high enough, the bubbles would oscillate in the liquid first as well and then collapse rapidly, indicating that the inertial cavitation occurs. However, when the intensity is insufficient to motivate the total bubble collapse, the bubbles in a liquid are compelled to oscillate in the acoustic field. Note that it is still controversial as to the question in which stage of the cavitation the nanobubbles are generated.

Intuitively, there are many instrument-related parameters, such as the ultrasonic time, the amplitude, the operating frequency, the tip size, and the input power, that could affect the cavitation dynamics and thus the nanobubble characteristics. Hereby, we do not intend to study the effects of all parameters but will focus primarily on the mechanism how the nucleation of the bulk nanobubbles depends on the ultrasonic time and amplitude. The pure water is treated under varying ultrasonic amplitude ranging from 20% to 40% and the ultrasonic time ranging from 5 min to 25 min. It should be noted that the nanoscale entities generated by the ultrasonication method were reported to be the gaseous nanobubbles based on a series of experimental tests[7, 27].

As shown in Fig. 5(a), both the ultrasonic amplitude A and the ultrasonic time t are generally proportional to the energy input E_{imput} of the instrument, and specifically, a linear dependence can be observed within the parameter ranges studied. During the ultrasonication, more energy input could create more nuclei in the finite-volume liquid, to excite more initial cavitation bubbles with a dramatic consumption of the dissolved gas molecules in the bulk (see Fig. 5(b)). Here we use the dissolved oxygen concentration DO, a frequently-used indicator of the gas content, to evaluate the consumption of the overall gas content in the solution. It can be seen that, the content of the dissolved gas in the nanobubble suspensions drops monotonously with the ultrasonic time and amplitude, and is about 8-18% lower than that in the pure water (DO ~7.6 mg/L). There is no additional gas input during the ultrasonic cavitation, suggesting that the consumed gas molecules either rise to the free surface within the large bubbles and collapse or reside in the bulk in the form of the bulk nanobubbles. The gas molecules accumulated inside the nanobubbles may be generated through the rectified diffusion from the bulk. Once nucleated, there could be a diffusion equilibrium between the gas within the nanobubbles and the bulk. Figure 5(c) shows the light scattering snapshots of two typical nanobubble samples captured by the NTA. With the prolonged sonication, more nanobubbles are detected and they are distributed uniformly in the bulk.

A quantitative comparison is shown in Fig. 4, with the size distribution profiles of the nanobubbles generated under different operating parameters. With the NTA system the size distribution of the nanobubbles with distinct properties can be accurately captured, along with the shapes pointing to a certain degree of the polydispersity. Here we have ensured that the video and analysis settings are consistent in all measurements to prevent introducing additional factors that could distort the analysis results. The sizes of the nanobubbles spread over a broad range (< 600 nm), with the main peak located in a range between 100 nm-200 nm. With the increase of the ultrasonic time (Fig. 6(a)) or amplitude (Fig. 6(b)), the number concentration N_b of the nanobubbles increases sharply and the dominate peak becomes more pronounced and shifts slightly to the smaller size side, for instance, down to ~100 nm.

It should be noted that recording for a sufficiently long period is significant to ensure the accuracy of the diffusion constants obtained by the NTA system. In this work, the Brownian motion of the bulk nanobubbles, in the form of scattering bright spots, is recorded at a framerate of 30 fps for at least

60 s. The duration of the measurements is far less than the long lifetime of the nanobubbles[11-12, 28]. The size variation of nanobubbles with time during the measurements could be ignored.

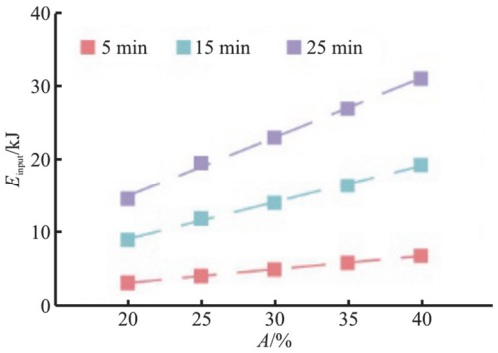

Fig. 5(a) (Color online) Effect of ultrasonic amplitude and ultrasonic time on energy input

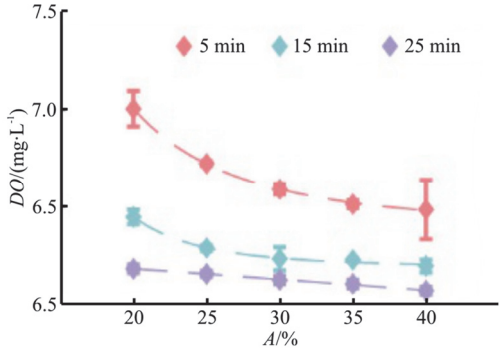

Fig. 5(b) (Color online) Dissolved oxygen concentration in bulk nanobubble suspensions prepared under different ultrasonic parameters (amplitude and time)

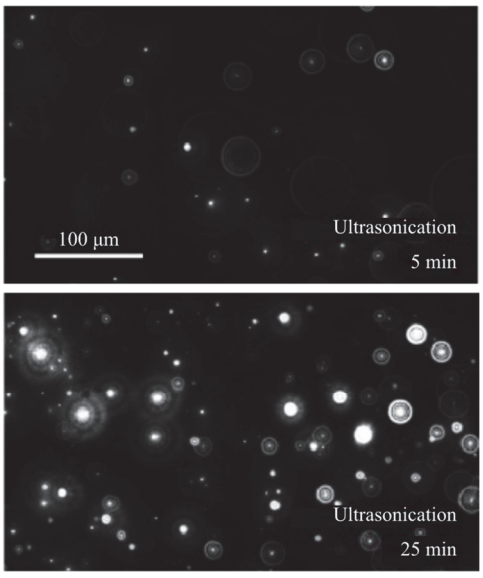

Fig. 5(c) NTA video frames showing two typical bulk nanobubble samples generated under ultrasonication 5 min, 25 min, respectively

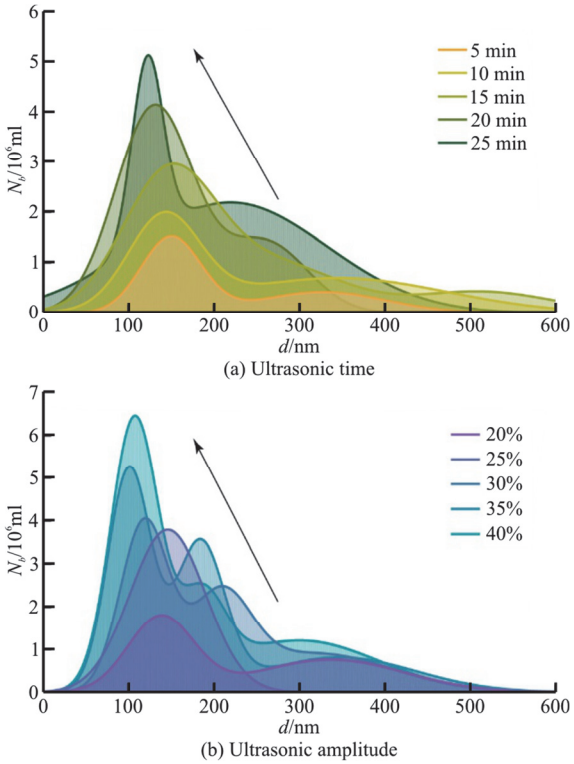

Fig. 6 (Color online) NTA-characterized size distributions of bulk nanobubbles generated under various

Having gained the size distribution of these nanobubble samples, the total number concentration and the mean bubble diameter can be calculated, as depicted in Fig. 7. Generally, a linear dependence between the number concentration and the ultrasonic amplitude/time, essentially the energy input, can be observed (Fig. 7(a)). For the mean diameter, both the NTA and the DLS are used for characterization. The mean bubble diameter D_b obtained by the NTA system lies in the range of 200 nm-300 nm (see Fig. 7(b)). As the ultrasonic amplitude or time increases, it decreases slightly as a whole. In contrast, the mean bubble diameter measured by the DLS technique is about 100 nm larger than that obtained by the NTA system, which once again verifies the bias of the DLS technique for the presence of a small number of large bubbles (see Fig. 7(c)). In view of a certain degree of polydispersity of the bulk nanobubbles, the NTA number-weighted measurement is more suitable for characterizing their properties than the DLS intensity-weighted measurements. Furthermore, it can be observed that the mean bubble diameter decreases slightly with the increase of the number concentration.

2.4 *Monitoring the thermodynamic response of bulk nanobubbles*

The intense research interest in the bulk nanobubbles stems from the scientific challenge of understanding their physical properties, especially, the

long-term stability. As a soft matter, the bulk nanobubbles could be sensitive to the physicochemical properties of the solutions, for instance, the pH value, the electrolyte, the ionic strength, and the presence of surfactant[25, 28]. We now turn our attention to the thermodynamic response of the bulk nanobubbles over a wide temperature range. The equipped temperature control module allows the NTA to track and analyze the nanobubble samples in the temperature range from 25°C (room temperature) to 70°C.

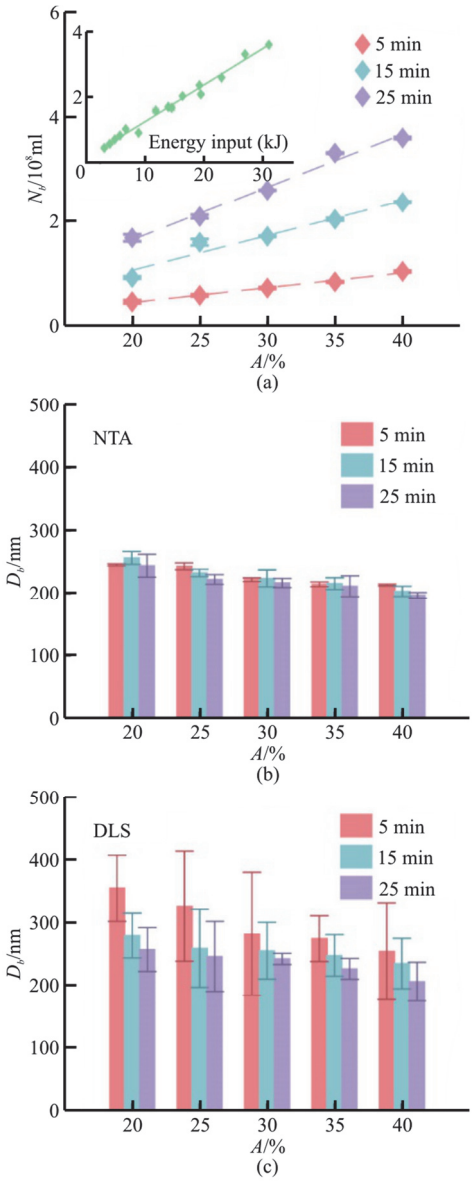

Fig. 7 (Color online) Characterization of bulk nanobubbles generated under various ultrasonic parameters. (a) Effect of ultrasonic amplitude and time on the total number concentration of bulk nanobubbles. The inset in (a) displays the number concentration of bulk nanobubbles as a function of energy input. Effect of ultrasonic amplitude and time on the mean diameter of bulk nanobubbles measured using (b) NTA and (c) DLS

Visualizing the formed nanobubbles, albeit only in the form of bright spots, using the NTA provides a rather complete overview of the dynamic behaviors. The bulk nanobubble suspensions are generated by the ultrasonication method under 25% amplitude. After loading and equilibrating for at least 30 min, the bulk nanobubble samples are measured with the NTA system under temperatures varying from 25°C to 70°C, which is consistent with the temperature range in our previous work measured with the DLS system[24].

The evolution of the bubble size distribution over a typical thermal cycle is shown in Fig. 8(a). It can be seen that, the bulk nanobubbles are quite sensitive to the ambient temperature T in which they survive, as manifested by a sharp narrowing of their size distribution. Interestingly, when the temperature exceeds ~45°C, it appears that the bubbles larger than 200 nm in diameter "disappear". Moreover, the peak diameter shifts continuously from ~150 nm to ~100 nm, while the number concentration remains almost constant (see Fig. 8(b)). This suggests that the temperature-sensitive properties of the bulk nanobubbles are a collective behavior with the shrinking of the large ones to specific sizes, which in turn produces a prominent main peak at high temperatures. This may suggest that both the interfacial properties of individual bubbles and the diffusive coupling effects of the bubble populations should be considered when rationalizing the stability of the bulk nanobubbles. It should be noted that, when analyzing these image sequences captured at different temperatures, we should take account of the effect of temperature on the parameters, such as the viscosity and the refractive index, and make corrections accordingly. Based on the size distribution, the mean bubble diameters at a given temperature are calculated to further quantify the thermodynamic response of the bulk nanobubbles to the temperature, as shown in Fig. 8(c)). One can see that the mean bubble diameter decreases sharply with the rising temperature up to about 45°C, above which it remains almost constant. The temperature dependence of the nanobubble size is universal for samples with concentrations ranging from 0.5×10^8 bubbles/mL to 2.1×10^8 bubbles/mL. The transition temperature determined in this experiment may not be applicable to the bulk nanobubbles generated by other methods, especially, in view of the type of the inside gas and the characteristics of the gas-liquid interface.

Overall, we demonstrate that, similar to the surface nanobubbles, the bulk nanobubbles can also withstand an increase of temperature up to at least 70°C without destabilization. Even more strikingly, the bulk nanobubbles exhibit good monodispersity at high temperatures, which could potentially benefit the medical and biological applications, such as the drug delivery. The NTA system exhibits the capacity to

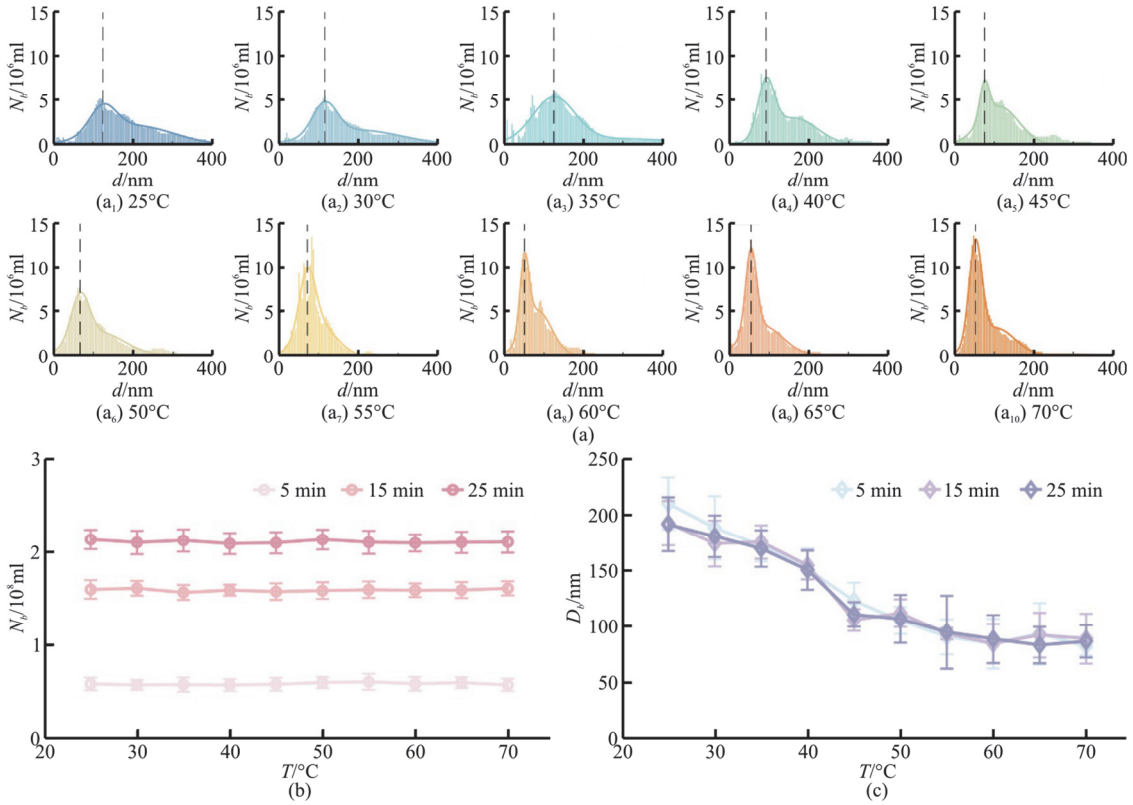

Fig. 8 (Color online) Effect of temperature on bulk nanobubbles. (a) Evolution of size distribution with temperature varying from 25°C to 70°C. In all cases, the bulk nanobubbles are generated in pure water for 15 min ultrasonic treatments and measured by the NTA techniques. (b) Effect of temperature on the bubble number concentration. (c) Effect of temperature on the bubble mean diameter. Error bars in each panel represent the standard deviation of six measurements

track and analyse the bulk nanobubbles *in situ*, substantially, their motion, even if these nano-objects are identified in the form of bright spots. It is helpful to systematically study the dynamic behavior of the bulk nanobubbles, such as the bubble destabilization, dissolution, and coalescence.

3. Conclusions

An NTA system is developed to characterize the Brownian diffusing particles of sizes ranging from ~20 nm to 1 000 nm under controlled conditions. Systematic testing with standard nanoparticles (20 nm-200 nm in diameter) is performed to confirm the good accuracy and resolution compared to the DLS technique. The NTA has the ability to visualize the nano-entities of sizes below the optical resolution limit, to obtain the number concentration and the size information by tracking and analysing individual particles. As far as the measurement principle is concerned, it has clear advantages in characterizing both the monodisperse and polydisperse nanoparticle populations, especially with the typical peak resolution. However, the NTA may be time-consuming compared to the DLS and requires some specialized manipulation skills to adjust the imaging and analysis settings for accurate results.

The anomalous stability is a puzzling property of the bulk nanobubbles, which makes it the focus of numerous fundamental researches. It is crucial to be able to determine the physical properties of the bulk nanobubbles under controlled conditions, and further rationalize their stability, as in contract to the classical Epstein-Plesset theory predictions. As an open and adjustable universal platform, the developed NTA is shown to be very suitable for tracking and characterizing the bulk nanobubbles. The nanobubble suspensions are produced using the ultrasonication method with different operating parameters (ultrasonic amplitude and time). It is shown that the nucleation of the bulk nanobubbles is facilitated by the increased ultrasonic treatment amplitude and time, essentially, the energy input, with a more concentrated size distribution, a higher number concentration, and smaller sizes. After the generation, the temperature control module of the NTA system makes it possible to monitor visually the thermodynamic response of the bulk nanobubbles over a wide temperature range from 25°C to 70°C. It is found that the bulk nanobubbles can survive a temperature up to 70°C without destabilizing or dissolving. With increasing temperature, they first shrink collectively and then remain constant with the transition temperature of around ~45°C. In this

work, we have primarily demonstrated the application of the NTA system in exploring the physical properties of the nanobubbles, without revealing the underlying stabilization mechanism. Further experiments are urgently required to solve this mystery.

Although only the temperature control module has been upgraded to the NTA system so far, some other major modifications, such as the pressure control, appear to be feasible and in the process of development. We expect a purpose-built, real-time, and user-friendly NTA system to be a reliable platform for studying the dynamic behavior of the bulk nanobubbles *in situ*, such as the coalescence and the collapse.

Compliance with Ethical Standards

Conflict of Interest: The authors declare that they have no conflict of interest.

Ethical approval: This article does not contain any studies with human participants or animals performed by any of the authors.

Informed consent: Informed consent was obtained from all individual participants included in the study.

References

[1] Tan B. H., An H., Ohl C. D. Stability of surface and bulk nanobubbles [J]. *Current Opinion in Colloid and Interface Science*, 2021, 53: 101428.

[2] Favvas E. P., Kyzas G. Z., Efthimiadou E. K. et al. Bulk nanobubbles, generation methods and potential applications [J]. *Current Opinion in Colloid and Interface Science*, 2021, 54: 101455.

[3] Zhang F., Sun L., Yang H. et al. Recent advances for understanding the role of nanobubbles in particles flotation [J]. *Advances in Colloid and Interface Science*, 2021, 291: 102403.

[4] Gao Y., Li M., Sun C. et al. Microbubble-enhanced water activation by cold plasma [J]. *Chemical Engineering Journal*, 2022, 446: 137318.

[5] Epstein P. S., Plesset M. S. On the stability of gas bubbles in liquid-gas solutions [J]. *The Journal of Chemical Physics*, 1950, 18(11): 1505-1509.

[6] Nirmalkar N., Pacek A. W., Barigou M. Bulk nanobubbles from acoustically cavitated aqueous organic solvent mixtures [J]. *Langmuir*, 2019, 35(6): 2188-2195.

[7] Nirmalkar N., Pacek A. W., Barigou M. On the existence and stability of bulk nanobubbles [J]. *Langmuir*, 2018, 34(37): 10964-10973.

[8] Tan B. H., An H., Ohl C. D. Identifying surface-attached nanobubbles [J]. *Current Opinion in Colloid and Interface Science*, 2021, 53: 101429.

[9] Lohse D., Zhang X. Pinning and gas oversaturation imply stable single surface nanobubbles [J]. *Physical Review E*, 2015, 91(3): 031003.

[10] Lohse D., Zhang X. Surface nanobubbles and nanodroplets [J]. *Reviews of Modern physics*, 2015, 87(3): 981.

[11] Wang Q., Zhao H., Qi N. et al. Generation and stability of size-adjustable bulk nanobubbles based on periodic pressure change [J]. *Scientific reports*, 2019, 9(1): 1-9.

[12] Sugano K., Miyoshi Y., Inazato S. Study of ultrafine bubble stabilization by organic material adhesion [J]. *Japanese Journal of Multiphase Flow*, 2017, 31(3): 299-306.

[13] Eklund F., Alheshibri M., Swenson J. Differentiating bulk nanobubbles from nanodroplets and nanoparticles [J]. *Current Opinion in Colloid and Interface Science*, 2021, 53: 101427.

[14] Bunkin N. F., Shkirin A. V., Ignatiev P. S. et al. Nanobubble clusters of dissolved gas in aqueous solutions of electrolyte. I. Experimental proof [J]. *The Journal of chemical physics*, 2012, 137(5): 054706.

[15] Alheshibri M., Craig V. S. J. Differentiating between nanoparticles and nanobubbles by evaluation of the compressibility and density of nanoparticles [J]. *The Journal of Physical Chemistry C*, 2018, 122(38): 21998-22007.

[16] Oh S. H., Kim J. M. Generation and stability of bulk nanobubbles [J]. *Langmuir*, 2017, 33(15): 3818-3823.

[17] Uchida T., Yamazaki K., Gohara K. Generation of micro- and nano-bubbles in water by dissociation of gas hydrates [J]. *Korean Journal of Chemical Engineering*, 2016, 33(5): 1749-1755.

[18] Filipe V., Hawe A., Jiskoot W. Critical evaluation of nanoparticle tracking analysis (NTA) by NanoSight for the measurement of nanoparticles and protein aggregates [J]. *Pharmaceutical research*, 2010, 27(5): 796-810.

[19] Gallego-Urrea J. A., Tuoriniemi J., Hassellöv M. Applications of particle-tracking analysis to the determination of size distributions and concentrations of nanoparticles in environmental, biological and food samples [J]. *TrAC Trends in Analytical Chemistry*, 2011, 30(3): 473-483.

[20] Van Der Pol E., Coumans F. A. W., Sturk A. et al. Refractive index determination of nanoparticles in suspension using nanoparticle tracking analysis [J]. *Nano letters*, 2014, 14(11): 6195-6201.

[21] Malloy A., Carr B. Nanoparticle tracking analysis–The halo™ system [J]. *Particle and Particle Systems Characterization*, 2006, 23(2): 197-204.

[22] Walker J. G. Improved nano-particle tracking analysis [J]. *Measurement Science and Technology*, 2012, 23(6): 065605.

[23] Wagner T., Lipinski H. G., Wiemann M. Dark field nanoparticle tracking analysis for size characterization of plasmonic and non-plasmonic particles [J]. *Journal of Nanoparticle research*, 2014, 16(5): 2419.

[24] Li M., Ma X., Eisener J. et al. How bulk nanobubbles are stable over a wide range of temperatures [J]. *Journal of Colloid and Interface Science*, 2021, 596: 184-198.

[25] Ma X. Li M., Pfeiffer P. et al. Ion adsorption stabilizes bulk nanobubbles [J]. *Journal of Colloid and Interface Science*, 2022, 606: 1380-1394.

[26] Brennen C. E. Cavitation and bubble dynamics [M]. Cambridge, UK: Cambridge University Press, 2014.

[27] Kim J. Y., Song M. G., Kim J. D. Zeta potential of nanobubbles generated by ultrasonication in aqueous alkyl polyglycoside solutions [J]. *Journal of Colloid and Interface Science*, 2000, 223(2): 285-291.

[28] Ghaani M. R., Kusalik P. G., English N. J. Massive generation of metastable bulk nanobubbles in water by external electric fields [J]. *Science advances*, 2020, 6(14): eaaz0094.